Geological Quarterly, 2015, **59** (2): 316–324
DOI: http://dx.doi.org/10.7306/gq.1223

The stability of xenotime in high Ca and Ca-Na systems, under experimental conditions of 250–350°C and 200–400 MPa: the implications for fluid-mediated low-temperature processes in granitic rocks

Bartosz BUDZYŃ[1, 2, *] and Gabriela A. KOZUB-BUDZYŃ[3]

[1] Polish Academy of Sciences, Institute of Geological Sciences, Research Centre in Kraków, Senacka 1, 31-002 Kraków, Poland

[2] Jagiellonian University, Institute of Geological Sciences, Oleandry 2a, 30-063 Kraków, Poland

[3] AGH University of Science and Technology, Faculty of Geology, Geophysics and Environmental Protection, al. A. Mickiewicza 30, 30-059 Kraków, Poland

Budzyń, B., Kozub-Budzyń, G. A., 2015. The stability of xenotime in high Ca and Ca-Na systems, under experimental conditions of 250–350°C and 200–400 MPa: the implications for fluid-mediated low-temperature processes in granitic rocks. Geological Quarterly, **59** (2): 316–324, doi: 10.7306/gq.1223

The stability of xenotime was tested by experiments in the presence of a silicate mineral assemblage and two different fluids, 2M $Ca(OH)_2$ or $Na_2Si_2O_5 + H_2O$, under P-T conditions of 200–400 MPa and 250–350°C. The xenotime was stable in runs with 2M $Ca(OH)_2$, replicating the low-temperature metasomatic alterations of granitic rocks, except in experiment at 350°C and 400 MPa, where some (Y,REE)-rich fluorapatite formed. Experiments with $Na_2Si_2O_5 + H_2O$ resulted in significant xenotime alteration and partial replacement by an unknown (Y,HREE)-rich silicate, and in the formation of minor amounts of (Y,REE)-rich fluorapatite. The latter indicate preferential partitioning of Y and REE into silicates over phosphates during low-temperature, metasomatic processes in a high Na-Ca system, similar to peralkaline granitic rocks.

Key words: xenotime, fluorapatite, yttrium silicate, rare earth elements, experimental petrology.

INTRODUCTION

Xenotime, $(Y,HREE)PO_4$, is an accessory mineral of granitic rocks, pegmatites, low- to high-grade metamorphic rocks, and migmatites (Förster, 1998). Xenotime is also present as detrital mineral in sedimentary rocks or as an authigenic phase, commonly formed on zircon in siliciclastic rocks (Fletcher et al., 2000; Rasmussen et al., 2004; Rasmussen, 2005). Because of its U and Th contents, xenotime has applications in isotopic U-Pb dating using mass spectrometry (Rasmussen et al., 2004; Rasmussen, 2005) and in chemical U-Th-total Pb dating using electron microprobe (Cocherie and Legendre, 2007; Hetherington et al., 2008; Suzuki and Kato, 2008). The application of microanalytical methods, such as sensitive high-resolution ion microprobe (SHRIMP) or electron microprobe, to date xenotime provides age data in textural context to constrain the age of particular igneous, metamorphic or diagenetic processes. Although xenotime is a relatively stable mineral, fluid-mediated alteration may lead to xenotime breakdown and replacement by Y-rich apatite and Y-rich epidote recognized in metamorphosed granitic rocks (Broska et al., 2005) or by fluorapatite and hingganite-(Y), documented in Skoddefjellet pegmatite from Svalbard (Majka et al., 2011). The P-T conditions of xenotime alterations are not tightly constrained, and experimental data are necessary to fully understand the stability of xenotime as a function of pressure-temperature conditions, accompanying mineral assemblage, and fluid composition.

Previous experimental works on xenotime focused on relatively simple systems. The stability of xenotime in the presence of common metamorphic and igneous fluids (H_2O, NaCl and KCl brines, $CaF_2 + H_2O$, 1M and 2M HCl, 1M and 2M H_2SO_4, 1M NaOH, and $Na_2Si_2O_5 + H_2O$) was tested at 500 MPa and 600°C, and 1000 MPa and 900°C, documenting the dissolution and etching of xenotime crystal faces, the formation of porous textures or the growth of small xenotime grains in some experiments – but no internal compositional alterations (Hetherington et al., 2010). The experiments at the same conditions of 500 MPa and 600°C, and 1000 MPa and 900°C, with starting compositions of xenotime + SiO_2 + Al_2O_3 + $ThSiO_4$ + $Na_2Si_2O_5$ + H_2O, resulted in compositional alteration of xenotime and enrichment in $ThSiO_4$ along rims (Harlov and Wirth, 2012), partially replicating the Th enrichment of xenotime in granitic pegmatites from the Hidra anorthosite, Norway (Hetherington and Harlov, 2008). Xenotime has also been tested for its solubility in H_2O and H_2O-NaCl fluids at 1 GPa and 800°C, showing higher solubility of YPO_4 than $CePO_4$ in pure H_2O to $X_{NaCl} = 0.27$

* Corresponding author, e-mail: ndbudzyn@cyf-kr.edu.pl

Received: December 3, 2014; accepted: January 8, 2015; first published online: February 25, 2015

and lower solubility with increasing NaCl concentration (Tropper et al., 2011). The experiments replicating systems of natural rocks, involving xenotime + albite + K-feldspar + biotite + muscovite + SiO_2 + CaF_2 with a variety of fluids, 2M KOH, 2M NaOH, 2M $Ca(OH)_2$ or $Na_2Si_2O_5$ + H_2O, ran under conditions of 450°C and 590 MPa, decreasing to 540 MPa over 16 days, resulted in xenotime alteration in all runs, with the formation of Y-rich britholite and fluorapatite (Budzyń and Harlov, 2011). There is a lack of published experimental works regarding the stability of xenotime in the presence of silicates and fluids replicating conditions of low-temperature metamorphism or hydrothermal, post-magmatic alterations in granitic rocks.

This study experimentally explores the stability of xenotime under conditions of 200–400 MPa and 250–350°C, in the presence of silicate minerals assemblages and fluid. Experiments with 2M $Ca(OH)_2$ alkaline fluid replicate conditions of the low-temperature metamorphism of granitic rocks. The second set of experiments, with $Na_2Si_2O_5$ + H_2O alkali fluid, shows Y and REE partitioning between phosphates and silicates, during the low-temperature metamorphic overprint of granites or during fluid-mediated post-magmatic processes in peralkaline granitic rocks.

EXPERIMENTAL AND ANALYTICAL METHODS

EXPERIMENTAL METHODS

The xenotime used for the experiments is a portion of the crystal from pegmatite from the North-West Frontier Province (NWFP), Pakistan, also used in previous experimental works by Hetherington et al. (2010), Budzyń and Harlov (2011), Harlov and Wirth (2012) and Budzyń et al. (2014). The other natural minerals used include gem-quality albite (Ab_{100}; Rožňava, Slovakia), labradorite ($An_{60}Ab_{27}Kfs_3$; Chihuahua, Mexico), sanidine (Eifel region, Germany), muscovite (pegmatite, Siedlimowice, SW Poland), biotite (gneiss, Sikkim Himalaya, India), and garnet (Gore Mountain, NY, USA). The chosen mineral compositions and used weight proportions (Table 1) roughly replicate that of granitic rock. Relatively high amounts of xenotime (ca. 5 mg of xenotime in ca. 34.6 to 40.0 mg total charge of capsule) were added to guarantee observation of xenotime in specimens with experimental products, because the material from each capsule was planned to be split between 3-4 portions. CaF_2 (Suprapure, Merck) was used in experiments in excess as a source of Ca and F to increase reaction rates, and to form fluorapatite. Synthetic SiO_2 was used instead of natural quartz to increase reaction rates. Garnet was added to test the fluid-mediated partitioning of Y between xenotime and garnet.

Crushed and sieved minerals to a fraction of 50–250 μm were washed in ethanol in an ultrasonic bath, and foreign or altered mineral grains were picked by hand under a binocular microscope. The fluids used included 2M $Ca(OH)_2$ and $Na_2Si_2O_5$ + H_2O, as they were the most aggressive fluids in previous experiments on monazite (Budzyń et al., 2011) and xenotime (Budzyń and Harlov, 2011). The minerals and reagents were weighed and mixed together while dry. The mixed solids were loaded into 3 mm wide, 15 mm long Au capsules, into which fluid was added using a syringe, which were then pinched shut. Then the capsules were arc-welded shut using a *Lampert PUK U3* argon plasma torch. Prior to runs, the capsules were checked for leaks by weighing, drying in a 105°C oven overnight, and then weighing again.

The experiments were conducted at the Deutsche GeoForschungsZentrum (Potsdam, Germany) using a standard cold-seal, 6 mm bore, René metal autoclaves with H_2O as the pressure medium. Four gently flattened capsules, two for xenotime experiments with 2M $Ca(OH)_2$ and $Na_2Si_2O_5$ + H_2O fluids, and two for "twin" experiments on monazite (Budzyń et al., 2013, 2015), were placed in each autoclave. Three sets of experiments were run under P-T conditions and with a duration of: (1) 200 MPa, 250°C, 40 days; (2) 200 MPa, 350°C, 40 days; and (3) 400 MPa, 350°C, 20 days (Table 1). Durations of the experiments were chosen based on previous experiments on the stabilities of monazite and xenotime (Hetherington et al., 2010; Budzyń and Harlov, 2011; Budzyń et al., 2011; Harlov et al., 2011). Pressures and temperatures were stable during the runs. At the end of the experiments, the autoclaves were cooled using compressed air, reaching temperatures of <100°C within <1 min. After the runs, the capsules were weighed, opened, and dried in a 105°C oven. The experimental products were mounted in epoxy and polished for electron microprobe analyses. The second portion was sprinkled on the SEM mount with adhesive carbon tape for back-scattered electron (BSE) imaging.

ANALYTICAL METHODS

The primary observations and analyses of the starting minerals and experimental products were performed using a Hitachi S-4700 field emission scanning electron microscope (SEM) equipped with an energy-dispersive spectrometer (EDS) at the Institute of Geological Sciences, Jagiellonian University (Kraków, Poland).

The chemical compositions of xenotime, (Y,REE)-rich fluorapatite, and unnamed (Y,HREE)-rich silicate were determined using a *Cameca SX 100* electron microprobe equipped with four-wavelength-dispersive spectrometers (WDS) at the Department of Special Laboratories, Laboratory of Electron Microanalysis, Geological Institute of Dionýz Štúr (Bratislava, Slovak Republic). The xenotime was analyzed under conditions of 15 kV accelerating voltage, 180 nA beam current, and 3 μm beam size, focused on the grain mount and coated with ca. 25 nm carbon film. The natural and synthetic standards, and the corresponding spectral lines used for standardization were as follows: apatite (P Kα), $PbCO_3$ (Pb Mβ), ThO_2 (Th Mα), UO_2 (U Mβ), YPO_4 (Y Lα), $LaPO_4$ (La Lα), $CePO_4$ (Ce Lα), $PrPO_4$(Pr Lβ), $NdPO_4$ (Nd Lα), $SmPO_4$ (Sm Lα), $EuPO_4$ (Eu Lβ), $GdPO_4$ (Gd Lα), $TbPO_4$ (Tb Lα), $DyPO_4$ (Dy Lβ), $HoPO_4$ (Ho Lβ), $ErPO_4$ (Er Lβ), $TmPO_4$ (Tm Lα), $YbPO_4$ (Yb Lα), $LuPO_4$ (Lu Lβ), fayalite (Fe Kα), barite (S Kα), wollastonite (Ca Kα, Si Kα), $SrTiO_3$ (Sr Lα), Al_2O_3 (Al Kα), and GaAs (As Lα). The counting times (peak/background, in sec.) were as follows: P 10/5, Pb 300/150, Th 60/30, U 30/20, Y 10/5, La 10/5, Ce 10/5, Pr 30/15, Nd 10/5, Sm 10/5, Eu 30/15, Gd 20/10, Tb 20/10, Dy 30/15, Ho 60/30, Er 60/30, Tm 30/15, Yb 30/15, Lu 100/50, Fe 20/20, S 10/10, Ca 20/10, Sr 20/10, Al 10/10, Si 10/10, and As 20/20. (Y,REE)-rich fluorapatite and unnamed (Y,HREE)-rich silicate were analysed using two conditions of: (1) 15 kV, 20 nA for F (30/15 sec), Si (10/5), Na (10/5), Al (10/5), Mg (10/5) P (10/5), Ca (10/5), K (10/5), Cl (10/5), Fe (10/5), Mn (10/5), Ti (10/5); followed by (2) 15 kV, 80 nA for Y (30/15), Sr (60/30), Pb (30/15), Ce (40/20), La (40/20), Nd (30/15), Pr (50/25), Sm (30/15), Eu (60/30), Gd (40/20), Tb (20/10), Dy (60/30), Th (30/15), U (40/20), and 1–5 μm beam size, depending on the size of the grain analysed.

Chemical analyses of silicates and compositional WDS X-ray maps of xenotime from experiments were performed us-

Table 1

Experimental conditions, starting materials (mg), and remarks

Experiment	*T* [°C]	*P* [MPa]	Duration (days)	Xtm	Ab	Lbr	Kfs	Bt	Ms	Grt	SiO_2	CaF_2	2M $Ca(OH)_2$	$Na_2Si_2O_5$	H_2O	Total charge	Solids added	Real charge	Mineral products	Remarks
X12C-04	250	200	40	5.14	–	4.01	3.20	4.00	2.11	4.02	4.23	3.07	0.75	–	5.22	35.75	29.80	35.02	Wo	Starting minerals are not altered. Wollastonite formed.
X12C-05	350	200	40	5.06	–	3.91	3.05	4.18	1.85	4.05	3.95	3.08	0.80	–	5.17	35.10	29.41	34.58	–	Minerals not altered, new phases not produced.
X12C-15	350	400	20	5.44	–	3.96	2.90	3.90	2.13	4.30	3.85	2.87	0.80	–	5.13	35.28	29.54	34.67	YAp	Delicate crystals of Y-bearing fluorapatite formed on the xenotime surface.
X12N-04	250	200	40	4.99	4.06	–	3.02	3.85	1.90	4.33	4.00	2.79	–	4.72	5.95	39.61	33.30	39.25	YAp, YSi, Amph	Delicate crystals of (Y,REE)-rich fluorapatite formed on the xenotime surface. K-feldspar is partially replaced by albite. Crystals of unnamed (Y,HREE)-rich silicate formed. Delicate needle-like crystals of amphibole are present.
X12N-05	350	200	40	5.04	4.02	–	3.13	3.97	1.93	3.93	3.86	2.91	–	5.02	5.43	39.24	33.21	38.64	YAp, YSi, Amph	Crystals of (Y,REE)-rich fluorapatite formed on the xenotime surface. K-feldspar is partially replaced by albite. High amounts of unnamed (Y,HREE)-rich silicate formed. Delicate needle-like crystals of amphibole are present.
X12N-15	350	400	20	5.34	3.90	–	3.42	3.75	2.06	4.52	4.06	3.25	–	4.92	5.44	40.66	34.55	39.99	YAp, YSi, Amph	Crystals of (Y,REE)-rich fluorapatite formed on the xenotime surface. K-feldspar is partially replaced by albite. Large crystals (reaching 200 μm across) of unnamed (Y,HREE)-rich silicate formed. Delicate needle-like crystals of amphibole are present.

"Total charge" and "solids added" represent original weights of materials; "real charge" represents lower values related to loss of solids during charging the capsule

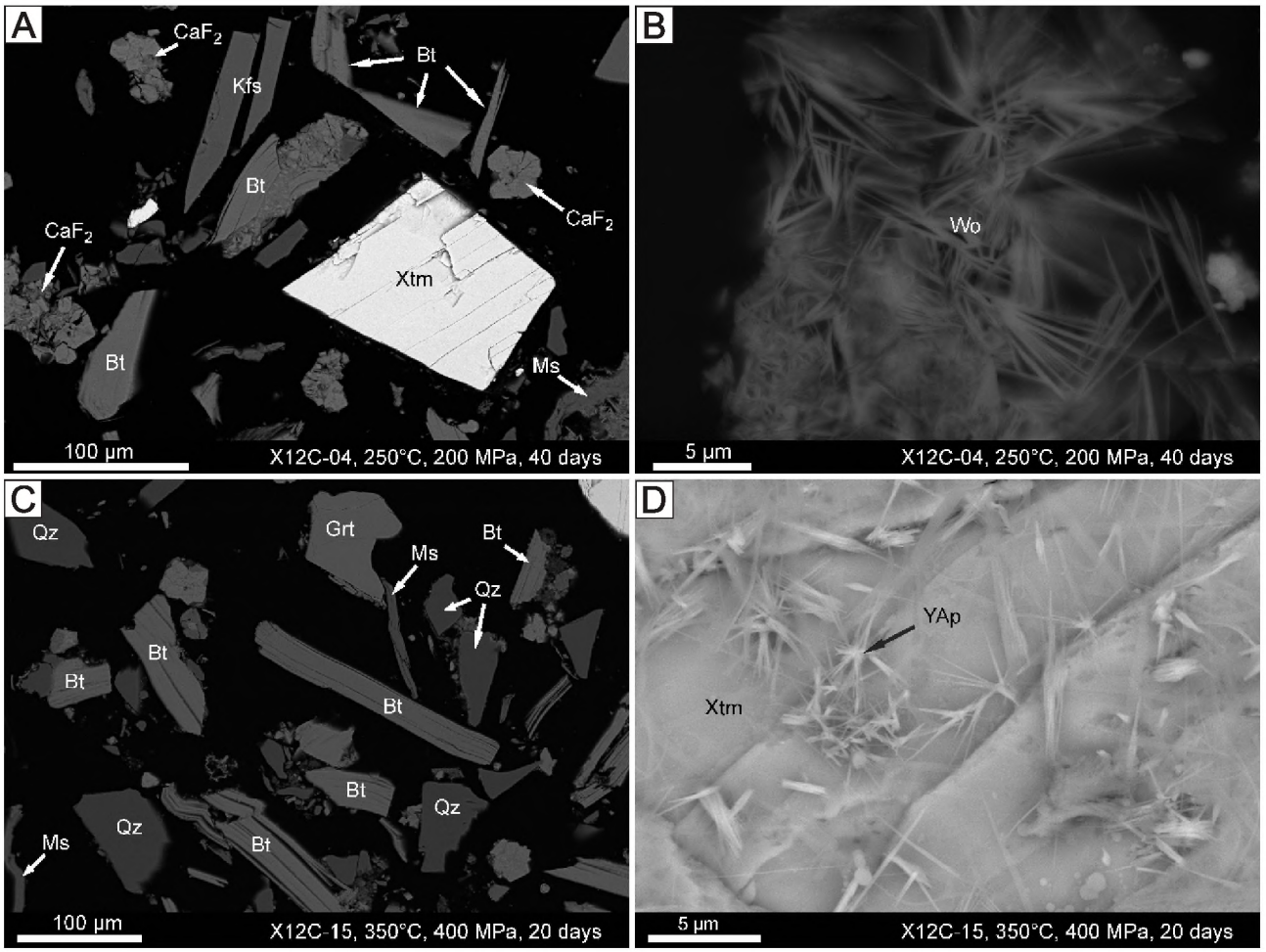

Fig. 1. Experimental products from runs with 2M $Ca(OH)_2$ fluid (BSE images)

A – xenotime, K-feldspar, biotite, and muscovite showing no signs of alterations in run at 200 MPa and 250°C; **B** – wollastonite formed in a run at 200 MPa and 250°C; **C** – unaltered silicates in products from runs at 400 MPa and 350°C; **D** – delicate, needle-like crystals of Y-bearing fluorapatite, formed on the xenotime surface in an experiment run at 400 MPa and 350°C; mineral names abbreviations: Bt – biotite, Grt – garnet, Kfs – K-feldspar, Ms – muscovite, Qz – quartz, Xtm – xenotime, YAp – Y-bearing fluorapatite

ing a *JEOL SuperProbe JXA-8230* electron microprobe equipped with five wavelength-dispersive spectrometers in the Laboratory of Critical Elements AGH-KGHM, at the Faculty of Geology, Geophysics and Environmental Protection, AGH University of Science and Technology (Kraków, Poland). The analyses were performed using 15 kV accelerating voltage, 20 nA beam current, and 5 µm beam size for feldspars, 3 µm for micas, and a focused beam for garnet. The counting times on peak/background (in sec.) were 20/10 for Si, and 10/5 for the other elements in feldspars and micas; 10/5 for all elements except 30/15 for Y in garnet. Compositional WDS X-ray maps were collected using conditions of 15 kV, 100 nA, 100 ms dwell time, 0.33 µm step size and 0.3 µm beam size.

RESULTS

EXPERIMENTS WITH XENOTIME AND 2M $CA(OH)_2$ FLUID

Xenotime and the other starting minerals in the experimental products from runs with 2M $Ca(OH)_2$ are not altered regarding textures and composition (Fig. 1A, C, Table 2 and Appendices 1–3*). Wollastonite is the only phase formed in the lowest P-T run at 200 MPa and 250°C (Fig. 1B). Delicate, needle-like crystals of Y-rich fluorapatite (identification based on the EDS analysis) are present on the xenotime surface in products of the 400 MPa and 350°C run (Fig. 1D).

EXPERIMENTS WITH XENOTIME AND $NA_2SI_2O_5 + H_2O$ FLUID

All experiments with $Na_2Si_2O_5 + H_2O$ resulted in xenotime alteration and in the formation of new phases (Fig. 2). The xenotime shows partial dissolution and some etching on the surface (Fig. 2B, F, K, L). The xenotime in experimental products shows no compositional variations compared to the starting NWFP xenotime (Table 2). Delicate crystals of (Y,REE)-rich fluorapatite are present on the xenotime surface (Fig. 2D–G) or form individual, pristine grains (Fig. 2O) in all experimental P-T ranges. (Y,REE)-rich fluorapatite shows high variations of REE content (Appendix 4), i.e. 21.97–22.16 wt.% $(Y+REE)_2O_3$ in X12N-05 (200 MPa, 350°C) vs. 6.42–12.85 wt.% $(Y+REE)_2O_3$ in X12N-15 (400 MPa, 350°C). These correspond to Ca and P variations of 32.86-37.81 wt.% CaO and 27.71-28.16 wt.% P_2O_5 (X12N-05), and 41.55–50.61 wt.% CaO and

* Supplementary data associated with this article can be found, in the online version, at doi: 10.7306/gq.1223

Table 2

Average results of the electron microprobe analyses of the xenotime

Sample	T [°C]	P [MPa]	Duration (days)	n	P_2O_5	SiO_2	ThO_2	UO_2	Y_2O_3	Pr_2O_3	Nd_2O_3	Sm_2O_3	Eu_2O_3	Gd_2O_3	Tb_2O_3	Dy_2O_3	Ho_2O_3	Er_2O_3	Tm_2O_3	Yb_2O_3	Lu_2O_3	SO_3	Total
Starting xenotime				38	35.56	0.27	0.09	0.11	40.43	0.16	0.14	0.66	0.48	3.60	1.04	8.00	1.34	4.72	0.71	3.44	0.51	<0.01	101.27
					0.20	*0.26*	*0.07*	*0.08*	*0.73*	*0.02*	*0.08*	*0.04*	*0.05*	*0.42*	*0.12*	*0.56*	*0.04*	*0.09*	*0.03*	*0.30*	*0.05*		
X12C-04	250	200	40	15	35.62	0.21	0.09	0.10	40.62	0.16	0.13	0.68	0.52	3.65	1.03	7.75	1.28	4.52	0.67	3.27	0.52	0.02	100.85
					0.28	*0.07*	*0.06*	*0.07*	*0.84*	*0.01*	*0.08*	*0.03*	*0.05*	*0.48*	*0.11*	*0.42*	*0.06*	*0.17*	*0.04*	*0.25*	*0.04*	*0.02*	
X12C-05	350	200	40	7	35.48	0.22	0.08	0.10	39.91	0.16	0.13	0.65	0.54	3.61	1.01	7.71	1.29	4.61	0.69	3.48	0.53	<0.01	100.19
					0.32	*0.09*	*0.06*	*0.07*	*1.09*	*0.02*	*0.09*	*0.03*	*0.05*	*0.63*	*0.14*	*0.48*	*0.05*	*0.21*	*0.05*	*0.50*	*0.06*		
X12C-15	350	400	20	13	34.62	0.24	0.11	0.13	39.18	0.16	0.17	0.66	0.51	3.50	0.99	7.65	1.31	4.64	0.71	3.62	0.53	<0.01	98.71
					0.25	*0.08*	*0.05*	*0.06*	*0.65*	*0.01*	*0.05*	*0.05*	*0.06*	*0.66*	*0.12*	*0.49*	*0.03*	*0.14*	*0.05*	*0.42*	*0.05*		
X12N-04	250	200	40	9	35.37	0.24	0.10	0.13	40.12	0.15	0.15	0.64	0.50	3.47	1.00	7.79	1.34	4.71	0.71	3.41	0.51	0.02	100.34
					0.36	*0.12*	*0.07*	*0.10*	*0.54*	*0.02*	*0.04*	*0.02*	*0.06*	*0.51*	*0.14*	*0.79*	*0.06*	*0.09*	*0.03*	*0.27*	*0.02*	*0.02*	
X12N-05	350	200	40	8	35.44	0.26	0.12	0.14	40.54	0.15	0.17	0.65	0.49	3.22	0.95	7.52	1.30	4.68	0.72	3.60	0.57	<0.01	100.51
					0.28	*0.07*	*0.03*	*0.04*	*0.63*	*0.02*	*0.03*	*0.03*	*0.04*	*0.32*	*0.08*	*0.52*	*0.04*	*0.19*	*0.05*	*0.39*	*0.04*		
X12N-15	350	400	20	9	34.61	0.20	0.08	0.09	38.94	0.15	0.17	0.65	0.50	3.62	1.06	8.16	1.35	4.65	0.71	3.36	0.49	<0.01	98.80
					0.23	*0.06*	*0.04*	*0.05*	*0.28*	*0.02*	*0.02*	*0.03*	*0.04*	*0.29*	*0.08*	*0.39*	*0.04*	*0.07*	*0.02*	*0.25*	*0.04*		

All values are given in wt.%, italic – standard deviation; values of components below detection limit of electron microprobe are not presented in the table; As_2O_5 < 0.06, Al_2O_3 < 0.10, La_2O_3 < 0.06, Ce_2O_3 < 0.08, FeO < 0.01, CaO < 0.01, SrO < 0.02, PbO < 0.03

36.01–37.90 wt.% P_2O_5 (X12N-15). The (Y,REE)-rich fluorapatite is characterized by a high fluorine content of 3.41–7.48 wt.% in X12N-05 and 3.26–6.12 wt.% in X12N-15. The small size of (Y,REE)-rich fluorapatite from the X12N-04 (200 MPa, 250°C) run prevented electron microprobe analyses.

Beside (Y,REE)-rich fluorapatite, an unnamed (Y,HREE)-rich silicate formed in all runs with $Na_2Si_2O_5 + H_2O$. The unnamed (Y,HREE)-rich silicate forms crystals with sizes of a few micrometres across and several to 50 μm long in 200 MPa experiments (250–350°C; X12N-04, X12N-05; Fig. 2H, I), tetragonal grains reaching 200 μm-across in the 400 MPa and 350°C run (X12N-15; Fig. 2N), or partially replaces xenotime (Figs. 2C, L, M, 3). The chemical composition also varies between experiments. The largest differences are noticed in Si content (Appendix 4), i.e. 67.05–73.68 wt.% SiO_2 (200 MPa, 250°C), 48.62–49.37 wt.% SiO_2 (200 MPa, 350°C) and 58.86–66.67 wt.% SiO_2 (400 MPa, 350°C), and Y concentrations 11.17–12.98 wt.% Y_2O_3 (200 MPa, 250°C), 20.20–22.00 wt.% Y_2O_3 (200 MPa, 350°C), and 11.08–12.09 wt.% Y_2O_3 (400 MPa, 350°C). The elevated Ca content of 1.70–2.42 wt.% CaO was noticed at 200 MPa and 350°C, vs. lower 0.08-0.37 wt.% CaO at 200 MPa, 250°C, and 0.21–0.54 wt.% CaO at 400 MPa, 350°C. The unnamed (Y,HREE)-rich silicate has relatively low concentrations of Th and U, i.e. <0.03–0.11 wt.% ThO_2, 0.04–1.49 wt.% UO_2 (200 MPa, 250°C), <0.03 wt.% ThO_2 and <0.04 wt.% UO_2 (200 MPa, 350°C) and <0.03 wt.% ThO_2, 0.39–2.11 wt.% UO_2 (400 MPa, 350°C). There were no fluorine or chlorine substitutes in the formed unnamed (Y,HREE)-rich silicate.

In all runs, K-feldspar was partially replaced by albite due to the albitisation process (Fig. 2J, M and Appendix 1). Delicate, needle-like crystals of Na, Fe, Mg, and Al-rich amphibole (identification based on EDS analyses) formed in all runs (Fig. 2B, O). The small size of amphibole prevented electron microprobe analyzes. The starting albite, garnet, and micas were not altered (Appendices 1–3).

DISCUSSION

The experiments show significant differences in xenotime stability, depending on fluid composition. The experiments with 2M $Ca(OH)_2$ were promising regarding the alteration of xenotime and the formation of secondary fluorapatite. Previous experiments, under conditions of 450°C and 590 MPa decreasing to 540 MPa over 16 days, and with starting materials of xenotime + albite + K-feldspar + biotite + muscovite + SiO_2 + CaF_2 + 2M $Ca(OH)_2$, resulted in partial dissolution of the xenotime grain surfaces, and in the formation of Y-rich britholite and fluorapatite (Budzyń and Harlov, 2011). Furthermore, recent experiments constraining the stability of xenotime, using the same starting materials as used in this work, reported xenotime alteration and the formation of (Y,HREE)-rich fluorapatite or (Y,HREE)-rich britholite in the presence of 2M $Ca(OH)_2$ fluid in the wide P-T range of 200-1000 MPa and 450–750°C, as well as the formation of (Y,HREE)-rich epidote at 800–1000 MPa and 650°C (Budzyń et al., 2014). Here, the experiments show that xenotime remains stable in the presence of alkaline fluid with high-Ca activity under experimental P-T conditions of 200 MPa and 250-350°C, representing the lowest P-T conditions of the metamorphism of granitic rock. However, the presence of (Y,HREE)-rich fluorapatite indicates that limited alteration of xenotime may occur under conditions of 400 MPa and 350°C.

In nature, progressive metamorphism may result in the gradual presence of xenotime. In lower greenschist to upper amphibolite facies metasedimentary rocks from the Paleoproterozoic Mount Barren Group (southwestern Australia), detrital xenotime is stable below 450°C, disappears during

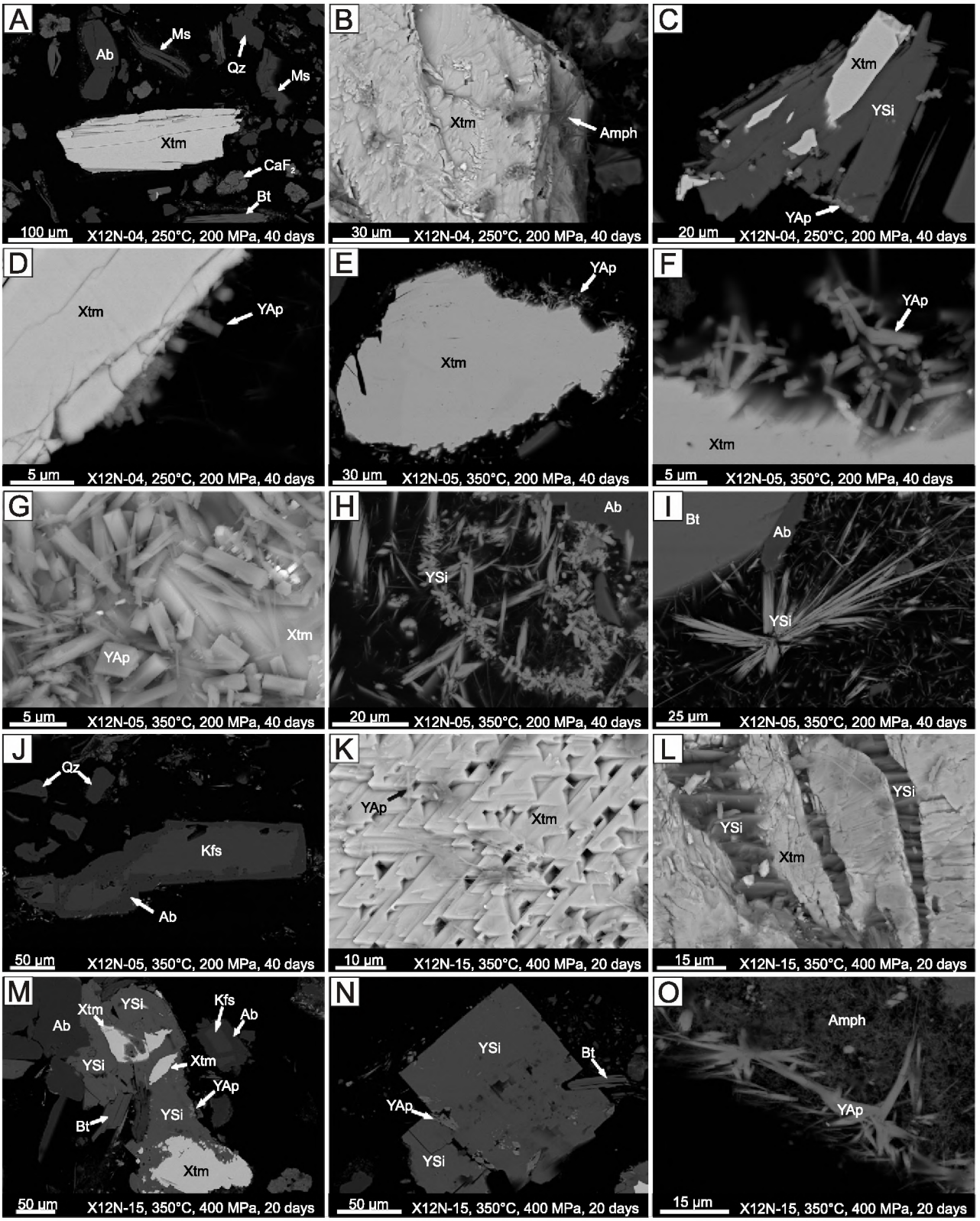

Fig. 2. Experimental products from runs with $Na_2Si_2O_5$ + H_2O fluid (BSE images)

A – unaltered minerals from an experiment at 200 MPa and 250°C; **B** – xenotime grains showing partial dissolution on the surface and delicate crystals of amphibole from runs at 200 MPa and 250°C; **C** – the unnamed (Y,HREE)-rich silicate replacing xenotime (200 MPa, 250°C); **D–G** – small crystals of (Y,REE)-rich fluorapatite formed on the xenotime surface in runs at 200 MPa and 250°C (D), and 200 MPa and 350°C (E–G); **H, I** – grains of the unnamed (Y,HREE)-rich silicate formed during an experiment at 200 MPa and 350°C; **J** – grain of K-feldspar with pseudomorphic replacement by albite along the rim due to an albitisation process; **K** – etched surface of the xenotime (400 MPa, 350°C); **L** – grains of the unnamed (Y,HREE)-rich silicate filling cracks of the xenotime (400 MPa, 350°C); **M** – xenotime partially replaced by the unnamed (Y,HREE)-rich silicate with the (Y,REE)-rich fluorapatite formed, and K-feldspar partially replaced by albite due to albitisation; **N** – large grains of the unnamed (Y,HREE)-rich silicate from 400 MPa and 350°C run; **O** – the (Y,REE)-rich fluorapatite and needle-like crystals of amphibole formed at 400 MPa and 350°C conditions; mineral names abbreviations: Ab – albite, Amph – amphibole, YSi – (Y,HREE)-rich silicate; other explanations as in Figure 1

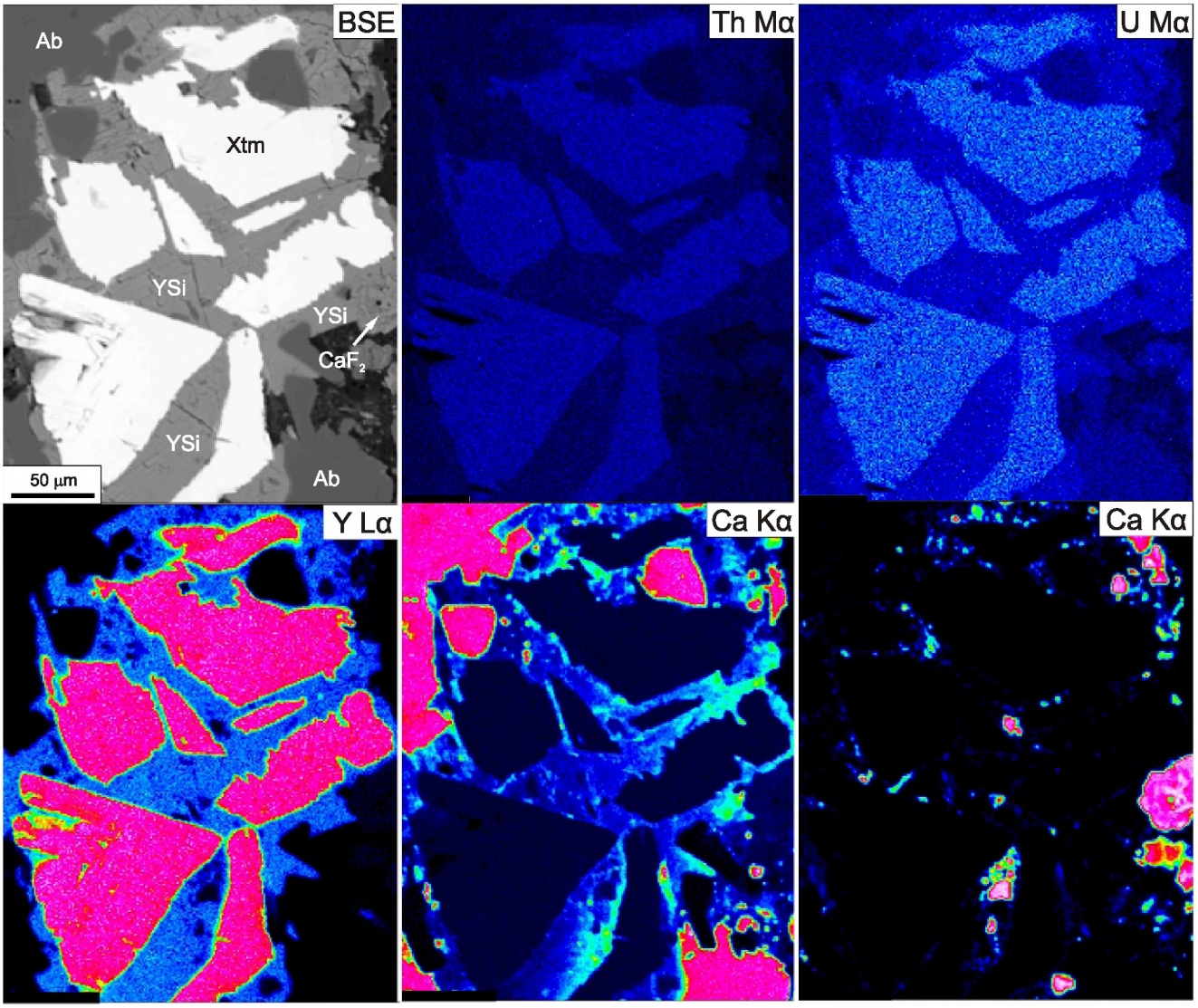

Fig. 3. BSE image and compositional WDS X-ray maps of the xenotime (Xtm) partially replaced by the unnamed (Y,HREE)-rich silicate (YSi) under conditions of 400 MPa and 350°C

Note that false enrichment of Y in grain boundaries of the xenotime and enrichment of Na and Ca in grain boundaries of the albite and CaF_2, respectively, are related to relief of grains in a polished grain mount; explanations as in Figure 2

the progressive metamorphism of pelites under mid-greenschist to amphibolite facies, and is present again under conditions of 650°C and ca. 8 kbar (Rasmussen et al., 2011). The growth of metamorphic xenotime was also documented on detrital xenotime under temperature conditions of 450°C in quartz-muscovite-chlorite schist (Rasmussen et al., 2011). The overgrowths were interpreted as resulting from compositional alterations or from the replacement of detrital xenotime by metamorphic xenotime, due to a fluid-mediated coupled dissolution-reprecipitation process (Rasmussen et al., 2011). The gradual presence of xenotime was also reported in Alpine metapelites. The temperature conditions of xenotime breakdown and the formation of secondary HREE-rich epidote and apatite were constrained to 450–528°C, with the disappearance of xenotime and co-existing monazite replaced by allanite or epidote in the biotite zone (Janots et al., 2008). The reversed reactions, i.e. allanite breakdown and the formation of monazite and xenotime, occurred at temperatures from 560 to 610°C, depending on the bulk CaO content and Ca/Na ratios (Janots et al., 2008). According to these works, xenotime is stable under temperature conditions below 450°C. The xenotime alterations related to fluid-mediated overprint were also reported in S-type granites affected by greenschist- to amphibolite facies metamorphism (Broska et al., 2005). The formation of secondary Y-rich apatite and Y-rich epidote rims around xenotime were documented in metamorphosed S-type granites, however, in low-Ca granites, the alteration of xenotime resulted in the formation of Y-enriched epidote, but not apatite (Broska et al., 2005). Our experimental setup had the bulk CaO content significantly increased in relation to that of the natural rocks due to labradorite, and high amounts of CaF_2 and 2M $Ca(OH)_2$ were used in excess to increase reaction rates. Despite the high availability of Ca, no epidote formed and limited formation of (Y,REE)-rich fluorapatite occurred only at 400 MPa and 350°C. The experimental results are consistent with observations in nature, showing that xenotime remains stable in a high-Ca system under conditions of 200–400 MPa and 250-350°C, with limited alteration at 400 MPa and 350°C.

There are limited experimental data on the stability of xenotime in the presence of the alkali fluid used in this work. Previous experiments, utilizing a simple system of xenotime and $Na_2Si_2O_5 + H_2O$ fluid, performed under high-grade conditions of 1000 MPa and 900°C, documented the dissolution of xenotime grain edges (Hetherington et al., 2010). Another study used a

mix of xenotime + ThO_2 + SiO_2 + Al_2O_3 and $Na_2Si_2O_5$ + H_2O fluid, resulting in $ThSiO_4$ enrichment along rims of xenotime grains under conditions of 500 MPa and 600°C, and 1000 MPa and 900°C (Harlov and Wirth, 2012). Because there was no source of other elements present in the natural rock system, the alteration mechanisms and formation of secondary phases were limited. In our study, the xenotime reacted in the presence of the alkali fluid and silicate minerals assemblage, roughly replicating granitic rock composition. Fluid-aided alterations resulted in dissolution of the xenotime surface (Fig. 2B, F, K), without affecting the composition of internal domains, similarly to the previous experiments from Hetherington et al. (2010). However, dissolved xenotime supplied P, Y, and HREE to form (Y,REE)-rich fluorapatite, while labradorite and CaF_2 were a source of the remaining Ca and F. It has to be noted that (Y,REE)-rich fluorapatite is not the main phase accumulating component released from the xenotime. The alkali fluid with high F activity promoted the mobility of Y and REE, incorporated in the unnamed (Y,HREE)-rich silicate that crystallised either as individual grains to grain aggregates (Fig. 2H, I, N) or formed subhedral to anhedral grains replacing the xenotime (Figs. 2C, L, M and 3). In the latter case, the unnamed (Y,HREE)-rich silicate, present along with the xenotime rims or inside xenotime grains, probably formed due to fluid penetration along cracks in the xenotime grains (Figs. 2L, M and 3). The alteration mechanism is interpreted as a pseudomorphic replacement, due to a fluid-mediated coupled dissolution-reprecipitation process (cf. Putnis, 2002, 2009; Harlov et al., 2011). There is also a distinct pattern of Y and REE substitution in the (Y,HREE)-rich silicate phase, showing similar concentrations of Y and REE in runs at 200 MPa and 250°C to 400 MPa and 350°C, and significant enrichment in Y and REE with an isobaric (200 MPa) temperature increase (250 to 350°C) from 11.08–12.98 to 20.20–21.27 wt.% Y_2O_3, and from 5.28–7.24 to 12.85–13.57 wt.% REE_2O_3. The composition of the unnamed (Y,HREE)-rich silicates is apparently variable and strongly depends on the P-T conditions.

An analogue of the (Y,HREE)-rich silicate phase in natural examples is difficult to find. Gerenite-(Y), $(Ca,Na)_2(Y,REE)_3Si_6O_{18}\cdot 2H_2O$, a rare mineral recognized in magmatic aplite-pegmatites from the Strange Lake peralkaline granitic pluton in northeastern Canada (Jambor et al., 1998), contains most of the cations as in the experimental products, however, its composition is very different. An unnamed (Y,HREE)-bearing hydrated silicate associated with turkestanite, $(Th,REE)(Ca,Na)_2K_{1-x}\square_x[Si_8O_{20}]\cdot nH_2O$, was described in peralkaline granites of the Morro Redondo Complex in Brazil (Vilalva and Vlach, 2010). Both phases are related to precipitation during the post-magmatic stage, in the presence of HFSE-rich fluids at temperature conditions of ca. 450°C (Vilalva and Vlach, 2010). The formation of a phase with a similar composition to turkestanite was experimentally achieved during the alteration of monazite in the presence of a silicate assemblage and $Na_2Si_2O_5$ + H_2O at 450-600 MPa and 450–500°C (Budzyń et al., 2011). The lower P-T experiments with monazite, silicates, and $Na_2Si_2O_5$ + H_2O fluid documented the formation of a phase with a composition similar to steacyite, $Th(Na,Ca)_2K_{1-x}\square_x[Si_8O_{20}]$, replacing monazite at 200–400 MPa and 250-350°C (Budzyń et al., 2013, 2015). The formation of fluorapatite incorporating Y and REEs released from experimentally-altered xenotime is limited, most likely due to the high availability of Si in the bulk system, promoting the formation of the unnamed (Y,HREE)-rich silicate in this study, or a Th- and LREE-bearing silicate phase in monazite experiments (Budzyń et al., 2013, 2015).

Xenotime, similarly to monazite, serves as a Th-U-Pb geochronometer, characterized by a high closure temperature. The volume diffusion of Pb in xenotime is extremely slow and experimentally constrained as slower than in zircon or monazite (Cherniak, 2006). The Pb loss in 40 μm grain at 800°C is estimated to ca. 5% of total Pb over 100 Ma (Cherniak, 2006). Similarly, the closure temperature limiting the volume diffusion of Pb in monazite is restricted to 800–900°C (Cherniak et al., 2004; Gardes et al., 2006). However, the fluid-aided alterations may cause the diffusion of REE, Th, U, and Pb in monazite, resulting in Th-U-Pb age disturbance (Teufel and Heinrich, 1997; Seydoux-Guillaume et al., 2002; Harlov et al., 2011; Budzyń et al., 2013, 2015) or a resetting of the Th-U-Pb ages (Williams et al., 2011). The mechanism of alterations leading to compositional modification in monazite is related to a fluid-aided coupled dissolution-reprecipitation process. Although concentrations of U, Th, and Pb in the NWFP xenotime were low, there were no notable changes after the experiments (Table 2). There are no modifications of Y and REE concentrations that may indicate alteration of the xenotime via a fluid-aided coupled dissolution-reprecipitation process, as documented in the experimental studies on monazite, including recent experiments using the same P-T conditions and duration (Budzyń et al., 2013, 2015). Taking these into account, as well as the excess of CaF_2 and fluid used to increase reaction rates, it is unlikely that a longer duration of experiments could significantly affect the stability of the xenotime. Summarizing, the experiments indicate that although alkali fluid mediates dissolution and partial replacement of the xenotime by secondary phases, the structure of xenotime prevents fluid infiltration from leading to compositional alteration of its internal domains.

CONCLUSIONS

The experiments regarding the stability of xenotime, together with corresponding experiments on monazite from Budzyń et al. (2013, 2015), provide important data on the partitioning of Y, REE, Th, and U between phosphates and silicates during low-temperature metasomatic processes.

1. Xenotime is stable in the presence of alkaline fluid with high Ca activity, showing limited alteration related to the formation of Y-rich fluorapatite under P-T conditions of 400 MPa and 350°C.

2. The experiments indicate that the formation of (Y,HREE)-rich silicates and (Y,REE)-rich fluorapatite can be related to low-temperature alteration of xenotime, mediated by alkali fluid with high Na activity. A large amount of the unnamed (Y,HREE)-rich silicates formed in the experiments indicates a preferential partitioning of Y and HREE into silicates, rather than phosphates, during low-temperature metasomatic processes.

3. The xenotime internal domains are not affected by compositional alteration in high Ca and Na-Ca systems, suggesting that xenotime can serve as a stable geochronometer in metasomatically altered rocks of granitic composition.

Acknowledgements. The analyses of the starting minerals were financially supported by the National Science Centre research grant number 2011/01/D/ST10/04588. This work was financially supported by the Institute of Geological Sciences, Polish Academy of Sciences as the research project “EXP”. B. Budzyń thanks W. Heinrich and D.E. Harlov for the access to the experimental laboratories of the Deutsche GeoForschungsZentrum, Potsdam, Germany. P. Konečný is thanked for his assistance with electron microprobe analyses. The reviews from I. Broska and R. Kryza, and editorial handling by T. Peryt are greatly acknowledged. M. Jastrzębski is thanked for his comments on an early version of this article.

REFERENCES

Broska, I., Williams, C.T., Janák, M., Nagy, G., 2005. Alteration and breakdown of xenotime-(Y) and monazite-(Ce) in granitic rocks of the Western Carpathians, Slovakia. Lithos, **82**: 71–83.

Budzyń, B., Harlov, D.E., 2011. The experimental alteration of xenotime in the presence of fluids and aluminosilicate minerals. Mineralia Slovaca, **42**: 173–174.

Budzyń, B., Harlov, D.E., Williams, M.L., Jercinovic, M.J., 2011. Experimental determination of stability relations between monazite, fluorapatite, allanite, and REE-epidote as a function of pressure, temperature, and fluid composition. American Mineralogist, **96**: 1547–1567.

Budzyń, B., Harlov, D.E., Konečný, P., 2013. Experimental, fluid-aided, low temperature mobilization of Y+REE and actinides between (Y+REE)-bearing phosphates and silicates. Mineralogia – Special Papers, **41**: 34.

Budzyń, B., Harlov, D.E., Majka, J., Kozub, G.A., 2014. Experimental constraints on the monazite-fluorapatite-allanite and xenotime-(Y,HREE)-rich fluorapatite-(Y,HREE)-rich epidote phase relations as a function of pressure, temperature, and Ca vs. Na activity in the fluid. Geophysical Research Abstracts, **16**: EGU2014-8583.

Budzyń, B., Konečný, P., Kozub-Budzyń, G.A., 2015. Stability of monazite and disturbance of Th-U-Pb system under experimental conditions of 250-350°C and 200-400 MPa. Annales Societatis Geologorum Poloniae, **85**: 405–425.

Cherniak, D.J., 2006. Pb and rare earth elements diffusion in xenotime. Lithos, **88**: 1–14.

Cherniak, D.J., Watson, E.B., Grove, M., Harrison, T.M., 2004. Pb diffusion in monazite: a combined RBS/SIMS study. Geochimica et Cosmochimica Acta, **68**: 829–840.

Cocherie, A., Legendre, A., 2007. Potential minerals for determining U-Th-Pb chemical age using electron microprobe. Lithos, **93**: 288–309.

Fletcher, I.R., Rasmussen, B., McNaughton, N.J., 2000. SHRIMP U-Pb geochronology of authigenic xenotime and its potential for dating sedimentary basins. Australian Journal of Earth Sciences, **47**: 845–859.

Förster, H.J., 1998. The chemical composition of REE-Y-Th-U-rich accessory minerals in peraluminous granites of the Erzgebirge-Fichtelgebirge region, Germany. Part II: Xenotime. American Mineralogist, **83**: 1302–1315.

Gardes, E., Jaoul, O., Montel, J., Seydoux-Guillaume, A.M., Wirth, R., 2006. Pb diffusion in monazite: an experimental study of Pb^{2+} + Th^{4+} - $2Nd^{3+}$ interdiffusion. Geochimica et Cosmochimica Acta, **70**: 2325–2336.

Harlov, D.E., Wirth, R., 2012. Experimental incorporation of Th into xenotime at middle to lower crustal P-T utilizing alkali-bearing fluids. American Mineralogist, **97**: 641–652.

Harlov, D.E., Wirth, R., Hetherington, C.J., 2011. Fluid-mediated partial alteration in monazite: the role of coupled dissolution-reprecipitation in element redistribution and mass transfer. Contributions to Mineralogy and Petrology, **162**: 329–348.

Hetherington, C.J., Harlov, D.E., 2008. Metasomatic thorite and uraninite inclusion in xenotime and monazite from granitic pegmatites, Hidra anorthosite massif, southwestern Norway: Mechanics and fluid chemistry. American Mineralogist, **93**: 806–820.

Hetherington, C.J., Jercinovic, M.J., Williams, M.L., Mahan, K., 2008. Understanding geologic processes with xenotime: composition, chronology, and a protocol for electron microprobe microanalysis. Chemical Geology, **254**: 133–147.

Hetherington, C.J., Harlov, D.E., Budzyń, B., 2010. Experimental initiation of dissolution-reprecipitation reactions in monazite and xenotime: the role of fluid composition. Mineralogy and Petrology, **99**: 165–184.

Jambor, J.L., Roberts, A.C., Grice, J.D., Birkett, T.C., Groat, L.A., Zajac, S., 1998. Gerenite-(Y), $(Ca,Na)_2(Y,REE)_3Si_6O_{18}\cdot 2H_2O$, a new mineral species, and an associated Y-bearing gadolinite-group mineral, from the Strange Lake peralkaline complex, Quebec-Labrador. Canadian Mineralogist, **36**: 793–800.

Janots, E., Engi, M., Berger, A., Allaz, J., Schwarz, J.-O., Spandler, C., 2008. Prograde metamorphic sequence of REE minerals in pelitic rocks of the Central Alps: implications for allanite–monazite–xenotime phase relations from 250 to 610°C. Journal of Metamorphic Geology, **26**: 509–526.

Majka, J., Pršek, J., Budzyń, B., Bačík, P., Barker, A., Łodziński, M., 2011. Fluorapatite-hingganite-(Y) coronas as products of fluid induced xenotime-(Y) breakdown in the Skoddefjellet pegmatite (Svalbard). Mineralogical Magazine, **75**: 159–167.

Putnis, A., 2002. Mineral replacement reactions: from macroscopic observations to microscopic mechanisms. Mineralogical Magazine, **66**: 689–708.

Putnis, A., 2009. Mineral replacement reactions. Reviews in Mineralogy and Geochemistry, **70**: 87–124.

Rasmussen, B., 2005. Radiometric dating of sedimentary rocks: the application of diagenetic xenotime geochronology. Earth-Science Reviews, **68**: 197–243.

Rasmussen, B., Fletcher, I.R., Bengston, S., McNaughton, N.J., 2004. SHRIMP U-Pb dating of diagenetic xenotime in the Stirling Range Formation, Western Australia: 1.8 billion year minimum age for the Stirling biota. Precambrian Research, **133**: 329–337.

Rasmussen, B., Fletcher, I.R., Muhling, J.R., 2011. Response of xenotime to prograde metamorphism. Contributions to Mineralogy and Petrology, **162**: 1259–1277.

Seydoux-Guillaume, A.M., Paquette, J.L., Wiedenbeck, M., Montel, J.M., Heinrich, W., 2002. Experimental resetting of the U-Th-Pb systems in monazite. Chemical Geology, **191**: 165–181.

Suzuki, K., Kato, T., 2008. CHIME dating of monazite, xenotime, zircon and polycrase: Protocol, pitfalls and chemical criterion of possibly discordant age data. Gondwana Research, **14**: 569–586.

Teufel, S., Heinrich, W., 1997. Partial resetting of the U-Pb isotope system in monazite through hydrothermal experiments: an SEM and U-Pb isotope study. Chemical Geology, **137**: 273–281.

Tropper, P., Manning, C.E., Harlov, D.E., 2011. Solubility of $CePO_4$ monazite and YPO_4 xenotime in H_2O and H_2O–NaCl at 800 °C and 1 GPa: Implications for REE and Y transport during high-grade metamorphism. Chemical Geology, **282**: 58–66.

Vilalva, F.C.J., Vlach, S.R.F., 2010. Major- and trace-element composition of REE-rich turkestanite from peralkaline granites of the Morro Redondo Complex, Graciosa Province, south Brasil. Mineralogical Magazine, **74**: 645–658.

Williams, M.L., Jercinovic, M.J., Harlov, D.E., Budzyń, B., Hetherington, C.J., 2011. Resetting monazite ages during fluid-related alteration. Chemical Geology, **283**: 218–225.